Multiple UV wavelength excitation and fluorescence of bioaerosols

Vasanthi Sivaprakasam, Alan L. Huston, Cathy Scotto and Jay D. Eversole

Optical Sciences Division, Naval Research Laboratory, Washington, DC 20375
sivaprak@ccs.nrl.navy.mil

Abstract: A two-wavelength laser-induced fluorescence technique is described for detecting and classifying biological aerosols. Single aerosols, smaller than 10 μm, are interrogated with 266 nm and 355 nm laser pulses separated in time by 400 ns. Fluorescence signals excited by these pulses are detected in three broad spectral bands centered at 350 nm, 450 nm and 550 nm. The results indicate that bacterial spores, vegetative bacterial cells and proteins can be differentiated based on the two wavelength excitation approach. Estimates of the fluorescence cross sections for 16 bioaerosol simulants and interferents are presented.

OCIS codes: (300.2530) Fluorescence, laser-induced, (290.5850) Scattering, particles

References and links

1. TSI Inc., 500 Cardigan Rd., Shoreview, MN, 55126-3996 (http://www.tsi.com).
2. J. Ho, "Future of biological aerosol detection," Analytica Chimica Acta **457,** 125-148 (2002).
3. V. Agranovski, Z. Ristovski, M. Hargreaves, P.J. Blackall and L. Morawska, "Real-time measurement of bacterial aerosols with the UVAPS: Performance evaluation," J. Aerosol Science **34,** 301-317 (2003).
4. C. A. Primmerman, "Detection of biological agents," Lincoln Laboratory Journal **12,** 3-32 (2000).
5. J.D. Eversole, W.K. Cary Jr., C.S. Scotto, R. Pierson, M. Spence and A.J. Campillo, Continuous bioaerosol monitoring using UV excitation fluorescence: Outdoor test results," Field Analytical Chemistry and Technology **15,** 205-212 (2001).
6. J.D. Eversole, J.J. Hardgrove, W.K. Cary Jr., D.P. Choulas and M. Seaver, "Continuous, rapid biological aerosol detection with the use of UV fluorescence: Outdoor test results," Field Analytical Chemistry and Technology **3,** 249-259 (1999).
7. C.R. Cantor and P.R. Schimmel, *Biophysical Chemistry* (W.H. Freeman, San Francisco, 1980) pp380, 443.
8. S.V. Konev, *Fluorescence and Phosphorescence of Proteins and Nucleic Acids* (Plenum, New York, 1967) P. 10.
9. T.D. Brock, M.T. Madigan, J.M. Martinko and J. Parker, *Biology of Microorganisms*, 7th ed. (Prentice Hall, Englewood Cliffs, NJ, 1994) Chap. 19.
10. Y. S. Cheng, E. B. Barr, B. J. Fan, P. J. Hargis, Jr., D. J. Rader, T. J. O'Hern, J. R. Torczynski, G. C. Tisone, B. L. Preppernau, S. A. Young and R. J. Radloff, "Detection of bioaerosols using multiwavelength UV fluorescence spectroscopy," Aerosol Science and Technology **30,** 186-201 (1999).
11. Duke Scientific Corporation. http://www.dukescientific.com
12. Gel-Tech (Now called Lightpath Technologies, no longer manufactures the sol-gel spheres)
13. Samples provided by AFIP were noted to include growth media.
14. G. W. Faris, R. A. Copeland, K. Mortelmans and B. V. Bronk, "Spectrally resolved absolute fluorescence cross sections for bacillus spores," Appl. Opt. **36,** 958-967 (1997).
15. M. Seaver, D.C. Roselle, J. Pinto and J. Eversole, "Absolute emission spectra from Bacillus subtillis and Escherichia coli vegetatative cells in solution," Appl. Opt. **37,** 5344-5347 (1998).

One of the advantages of the ultraviolet laser-induced fluorescence (UV-LIF) detection approach is that the cross sections for particles in the 1–10 μm range are sufficiently large to make single particle interrogation feasible. This high sensitivity has motivated development of several UV-LIF-based systems as front-ends or "triggers" for biological agent aerosol detectors as reported in scientific journals, e.g.,: the Ultraviolet-Aerodynamic Particle Sizer (UV-APS) manufactured by TSI, Inc. [1], the Fluorescence Aerodynamic Particle Sizer

#4798 - $15.00 US Received 14 July 2004; revised 7 September 2004; accepted 9 September 2004

(FLAPS) developed by the Canadian Defense ministry [2, 3], the Biological Agent Warning Sensor (BAWS), developed by MIT Lincoln Laboratory [4], and the Single Particle Fluorescence Analyzer (SPFA) developed at the Naval Research Laboratory [5, 6]. Typically, these types of systems have employed laser excitation sources that are now readily available commercially; utilizing either the third harmonic wavelength (349 nm) of a Nd:YLF (UV-APS and FLAPS), or 266 nm light from quadrupled Nd:YAG (BAWS and SPFA).

These two different excitation wavelengths probe different chromophores in target biological materials. For example, 266 nm excites the aromatic amino acids, tyrosine, tryptophan, and phenylalanine that each have characteristic emission bands between 300 nm and 400 nm [7, 8]. These natural chromophores are somewhat universal markers for biological materials since these amino acids will be present to some extent in nearly all proteins. Furthermore, the fluorescent cross section for tryptophan is relatively high compared to other specific biogenic chromophores. Fluorescence at longer (visible) wavelengths has been frequently attributed to reduced nicotinamide adenine dinucleotide (NADH), associated with cell metabolism, and flavins, such as riboflavin; although there are other biogenic compounds such as carotenoids and chlorophylls that also fluoresce [9]. The 349 nm excitation wavelength was originally chosen to excite biogenic chemicals associated with cell metabolism, such as NADH [2], and riboflavin which have characteristic broad emission bands peaked at 450 nm and 560 nm, respectively [2, 9]. However, the chemical origin of visible band emission from bacterial spores has remained somewhat mysterious since, by their nature, bacterial spores exist in a nearly dormant state with almost no metabolic activity and therefore do not contain much NADH or riboflavin [3]. It is now reasonably well known that fluorescence spectra of different types of bacteria are very similar, and that actual species-level identification based on these spectra is unlikely [10].

The task of detecting biological agents using fluorescence is complicated by interferences from both non-biological aerosols that contain aromatic hydrocarbons, such as industrial chemicals and engine exhausts, and indigenous biological aerosols, such as fungi, pollens, dander and bacteria that may be normally present in the environment. Although 266 nm is an effective pump for protein emission, the shorter wavelength may also be more likely to encounter a greater number of naturally occurring fluorescent non-biological aerosols. While the UV-LIF techniques developed so far appear to be reasonably efficient in distinguishing between non-fluorescent inorganic particles and fluorescent particles, they do not have a capacity for discriminating between potential threats and non-threats among those aerosols that do fluoresce significantly.

In this paper, we describe a new fluorescence-based bioaerosol detection approach that utilizes two different sequential UV excitation wavelengths to excite the same individual aerosol and detect the fluorescent signature from each excitation separated in time. Our goal is to determine if this improves the bioaerosol discrimination capabilities compared to single excitation wavelength systems. Our approach explores the possibility that different classes of biological aerosol materials, such as vegetative cells, spores and proteins, might be differentiated on the basis of both emission and excitation spectroscopy. In this paper, we have characterized the responses of sixteen types of aerosol samples, and established that within this sample set, spectral correlations exist based on the relative and absolute fluorescence intensities.

#4798 - $15.00 US Received 14 July 2004; revised 7 September 2004; accepted 9 September 2004

The optical components of the multiple wavelength excitation bio-aerosol detection system are shown schematically in Fig. 1. Micron-sized aerosols were generated using a

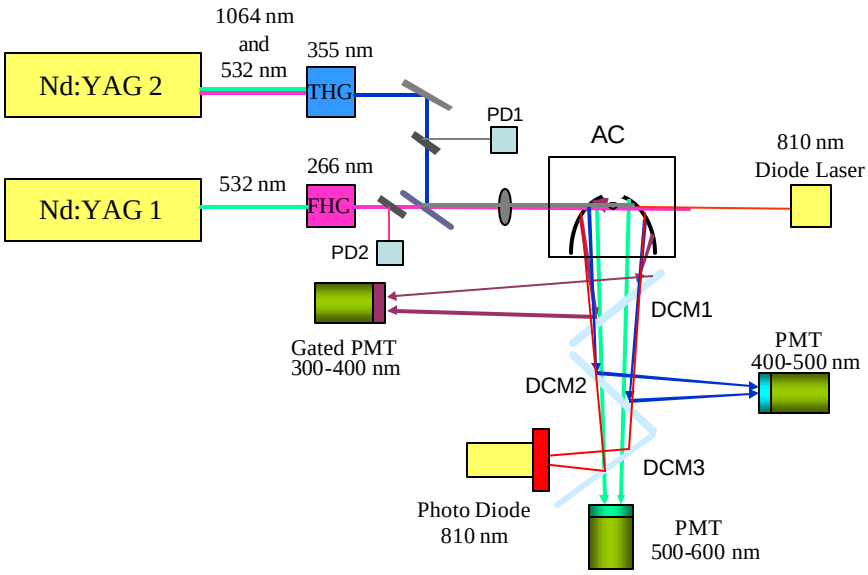

Fig. 1. Schematic of the experimental apparatus used for multiwavelength fluorescence excitation of bioaerosol particles. AC: aerosol chamber; Nd:YAG 1: laser 1, 5 nsec pulses at 1064 nm and 532 nm; THG: third harmonic generator output at 355 nm; Nd:YAG 2: laser 2, 20 nsec pulses at 1064 nm and 532 nm, FHG: fourth harmonic generator output at 266 nm; BS1 beam splitter, 8% reflection at 355nm; BS2: 8% reflection at 266nm; PD1: 355 nm power monitor photodiode; PD2: 266 nm power monitor photodiode; DCM1: dichroic beam splitter reflects 350 nm; DCM2 dichroic beam splitter reflects 450 nm; DCM3: dichroic beam splitter reflects 810 nm.

three-jet Collison nebulizer. These particles were directed through a nozzle into an aerosol chamber. The nozzle restricted the aerosols to a cylinder-shaped flow that is approximately 0.5 mm in diameter, and was positioned to direct the flow through the focal point of an elliptical mirror inside the chamber. A continuous wave (cw) 810 nm diode laser was focused to intercept aerosol particles at the focal position of the mirror. Light scattered by individual particles passing through this beam was efficiently collected and refocused onto an avalanche photodiode by the elliptical mirror. The light scattering signals were used to estimate the size of the aerosol particles, and to generate a cue signal for the pulsed excitation lasers when the scattering intensity exceeded a predetermined threshold. The output of the first laser occurred 1.2 μs following the cueing and the second laser pulse was generated approximately 0.4 μs after the first pulse. Between the time of the cue pulse and the second laser pulse, the particle traveled only about 110 μm.

Two, externally Q-switched, diode pumped Nd:YAG lasers were used to generate the UV excitation pulses (Coherent Model 501QDII and Coherent Vector 532-1000-20). The first laser was frequency-quadrupled to generate a 266 nm pulse having a 20 ns pulse width and the second laser was frequency-tripled to generate a 5 ns duration, 355 nm pulse. Fused silica

#4798 - $15.00 US Received 14 July 2004; revised 7 September 2004; accepted 9 September 2004

beam splitters were used to pick off a fraction of each pulse to monitor the energy using a pair of photodiodes. Both lasers were collinearly directed into the aerosol chamber and focused to a ~ 700 μm diameter waist to intercept the particle flow. The aerosol fluorescence was collected with an efficiency of nearly 2π steradian by the elliptical mirror, and was directed through a series of three custom dichroic beam splitters that separated the fluorescence into three broad wavelength bands. Photomultiplier tubes (PMT's) were used to detect the fluorescence signals in each of the three wavelength bands. The first beam splitter was designed to reflect light in a 70 nm wide band centered at 350 nm. A Hoya U360 color-glass filter was subsequently used to block any scattered 266 nm excitation, and a Schott S-8612 color-glass filter removed residual near-infrared light from the 810 nm diode laser. The second beam splitter reflected light passed by the first in a 80 nm band centered at 450 nm. A set of high-pass and low-pass interference filters was used to isolate the light in the 450 nm band. The third dichroic beamsplitter reflected light in a narrow band centered at 810 nm into an avalanche photodiode to monitor the elastic scattering. Any fluorescent emission in a 100 nm wide band, centered around 550 nm, passed through all the beam splitters to the third PMT. The PMT's for the 450 nm and 550 nm fluorescence bands were Hamamatsu models H5783-03 and H6780-02, respectively. The 350 nm band fluorescence detector, a Hamamatsu H7680-01, was gated to be on only when the 266 nm pulse was present. Gating prevented damage to the PMT by scattered light from the high intensity 355 nm laser. A four-channel, 1 GHz bandwidth storage oscilloscope was used to digitize the signals in this set of experiments. Each interrogated particle therefore generated eight independent data values: one elastic scatter intensity, five fluorescence emission intensities and two laser pulse intensity photodiode outputs.

The bioaerosol detection system was calibrated using a set of NIST-traceable, spherical polystyrene/latex (PSL) particles with diameters ranging from 0.9 μm to 7.0 μm [11]. Pure silica spheres with diameters of 0.9 μm and 2.3 μm were also used to characterize the response of the system [12]. The silica particles were manufactured using sol-gel techniques that assure a very high degree of purity thereby minimizing fluorescence. The aerosol sizes, as generated by the Collison nebulizer, were confirmed using a TSI 3220 Aerodynamic Particle Sizer. The silica spheres showed low fluorescence in all three of the wavelength bands. These low signal levels were just slightly higher than signals recorded when no particle was present in the chamber. Therefore these particles were used to establish the background noise level of the system. In this way, noise contributions to the recorded signals in the fluorescence channels due to elastic scattered light from the particle, secondary scattering from the walls of the aerosol chamber, and any intrinsic fluorescence from the optical components were taken into account. The 266 nm-excited un-doped PSL spheres had fluorescence signals in the 350 nm band that were more than an order of magnitude more intense than the silica spheres.

In order to establish the size response of our LIF system, the 810 nm elastic scattering signal and the 350 nm fluorescence signals were measured for 500 consecutive particles for a series of un-doped PSL particles ranging in size from 1 μm to 7 μm. As shown in Fig. 2, a power function fit to the averaged scatter signal data yielded a dependence that is proportional to the particle diameter raised to the power of 1.7, while the fluorescence intensity of the 350 nm fluorescence band was best fit by a slightly higher exponent of 2.1. Therefore within the

#4798 - $15.00 US Received 14 July 2004; revised 7 September 2004; accepted 9 September 2004

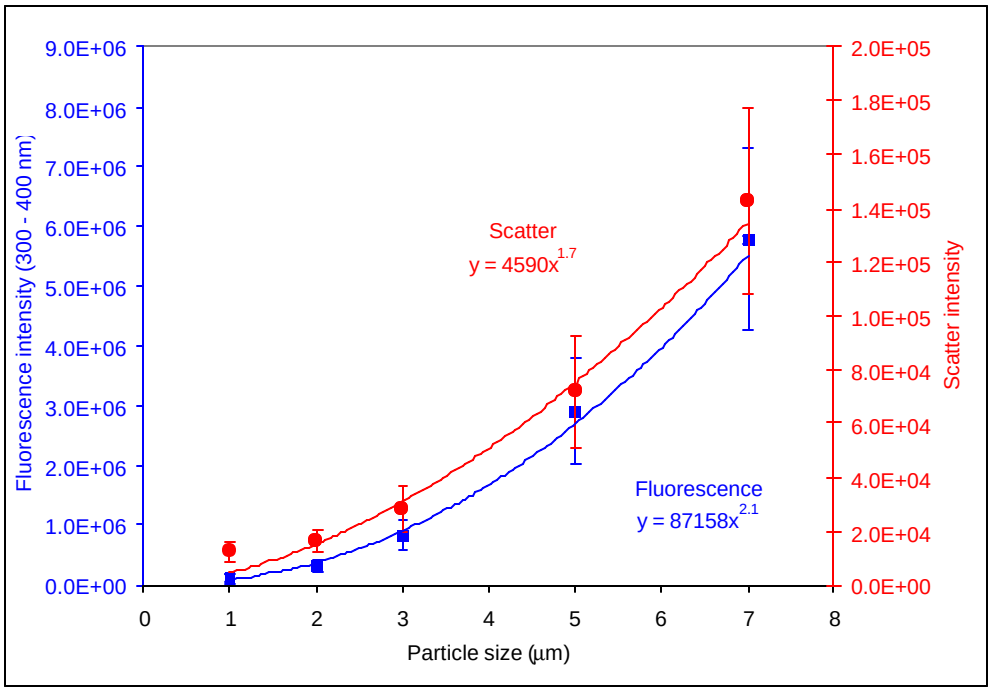

Fig. 2. Plots of the elastic scattered light and fluorescence intensity as a function of particle size for un-doped polystyrene spheres showing a cross-sectional area dependence on particle size.

precision of the measurements, both the fluorescence and scattering signals appear to scale as the geometric cross section of the particle.

A set of sixteen samples was investigated for this initial study to characterize the performance of the multi-wavelength excitation system. The samples are listed in Table 1, and include bacterial spores, vegetative bacterial cells, proteins, a fungal spore and kaolin clay. Both washed and unwashed biological samples were used. Unwashed samples were reported to contain significant amounts of growth media [13]. The table lists some of the characteristics of the samples and the rationale for including them in this initial study. Samples of Bacillus atrophaeus spores (usually referred to as BG, after its former name, bacillus globigii) were obtained from either Dugway Proving Ground, UT or Armed Forces Institute of Pathology (AFIP), Bethesda, MD.

Table 1. List of the simulants and interferents investigated

Sample	***Characteristics***	***Purpose***
Bacillus Cereus	Veg. Bac. Cells: G-pos rod	B. Anthracis simulant
Bacillus Subtilis	Veg. Bac. Cells: G-pos rod	B. Anthracis simulant
Bacillus Thuringiengis	Veg. Bac. Cells: G-pos rod	Insecticide/ Interferent
Micrococcus Luteus	Veg. Bac. Cells: G-pos cocci	Airborne interferent
Bacillus Megatarium	Veg. Bac. Cells: G-pos	B. Anthracis interferent
Brucella Neotomae - 0.9% NaCl	Veg. Bac. Cells: G-neg rods	Brucella sim. Brucellosis
Yersinia Rohdei – spent media	Veg. Bac. Cells: G-neg rods	Y-Pestis simulant / Plague
Pantoea Agglomerans – spent TSB media	Veg. Bac. Cells	Plant pathogen/tularensis

#4798 - $15.00 US Received 14 July 2004; revised 7 September 2004; accepted 9 September 2004

MS2 Phage – spent TSB media	Virus with e-coli debris	Virus
AFIP BG spores – spent G media	Bacterial Spores	B. Anthracis simulant
Dugway BG spores – unwashed	Bacterial Spores	B. Anthracis simulant
Dugway BG spores – washed	Bacterial Spores	B. Anthracis simulant
Ova Albumin	Protein	Toxin simulant
Albumin, Bovine Serum	Protein	Toxin simulant
Sporisorium Cruentum	Fungus	Interferent
Kaolin	Aluminosilicate clay	Inorganic interferent

The average scatter and the fluorescence signals obtained for the 16 samples are shown in Fig. 3. These data sets are presented as bar graphs depicting the relative average intensities measured from 500 consecutive particles of each sample type, the first bar corresponds to the scatter signal measured at 810 nm, the next 3 bars correspond to the 266 nm-excited fluorescence in the 350 nm, 450 nm and 550 nm bands, and the last two bars correspond to the 355 nm-excited fluorescence in the 450 nm and 550 nm bands. The error bars represent the standard deviation of the measurements for each data channel. Due to the large differences in fluorescence intensities in the different wavelength bands, the vertical scale of the bar plots is logarithmic. The measured signal pulses were integrated, and the resulting photocurrents were converted to incident intensities by correcting for the quantum efficiency and gain of the PMT provided by the manufacturer specifications. To correct for incident laser pulse intensity variations ($\pm$ 20% per pulse), the particle emission intensities were normalized by the ratio of their measured laser pulse intensity to the average laser pulse intensity. Next, the individual emission intensities were corrected for the transmittances of the individual optical elements for each beam path including an estimated collection efficiency of the elliptical mirror to yield number of photons emitted by the particle. Finally, the absolute fluorescence intensity of a given particle composition will depend on its size. Therefore each set of fluorescence signals from every particle was normalized to its elastic scatter intensity, as these two signals are expected to scale similarly with particle size as shown in Fig. 2. In order to represent the data as numbers of photons, these ratios were then multiplied by the elastic scatter intensity of a 1 micron diameter PSL particle. This yields the corrected emission intensities expressed as fluorescence signal emitted by an equivalent 1 μm particle for the purpose of comparing the relative emission intensity patterns of the different sample materials in Fig 3.

One point worth mentioning is that we are using the relationship between particle size, elastic scatter and fluorescence intensity established for polystyrene spheres to correct for the size dependence of the samples investigated in this study, while this relationship may not hold for biological samples. Further study is planned to study this relationship for varying size spores and vegetative cells. Most of the particles included in this study ranged in size around 1 μm, except for sporisorium cruentum which showed a distribution around 6 μm, thus making the normalizing to size a less critical factor.

The scatter and fluorescence signals for the washed vegetative cells are shown in row (a) of Fig. 3, vegetative cells in media and proteins are shown in row (b) and the signal for the various BG spores, the fungal spore and kaolin dust samples are shown in row (c). As can be seen from the data in row (a), the signals from the various washed vegetative cells show similar trends, the fluorescence emission is predominantly in the 350 nm band and is about

#4798 - $15.00 US Received 14 July 2004; revised 7 September 2004; accepted 9 September 2004

1.5 orders of magnitude higher than the fluorescence signal in the long wavelength bands. In contrast the vegetative cells in media show higher contribution to the fluorescence in the 450

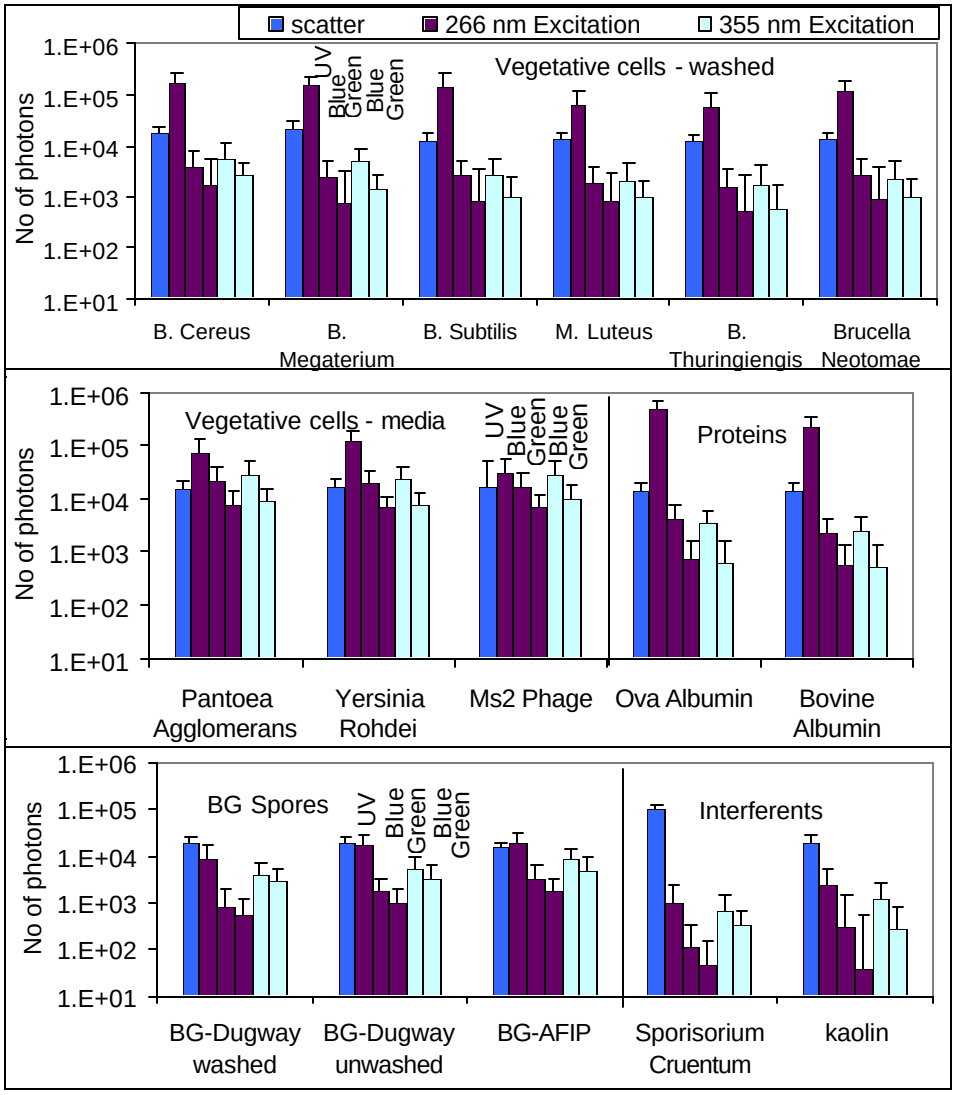

Fig. 3. Aerosol scattering and fluorescence data summary for the 16 samples listed in Table 1. The bars represent the average value obtained from 500 sequential records. There are six signals recorded for each particle: (a) scattered light intensity in arbitrary units; (b) 266 nm-excited 350 nm fluorescence signal; (c) 266 nm-excited 450 nm fluorescence signal; (d) 266 nm-excited 550 nm fluorescence signal; (e) 355 nm-excited 450 nm fluorescence signal; (f) 355 nm-excited 550 nm fluorescence signal. The fluorescence signal intensities are given in terms of the number of detected photons.

nm and the 550 nm bands for both excitation wavelengths. The BG spores show weaker emission compared to the vegetative cells, but the 355 nm excited fluorescence in the 450 nm and the 550 nm bands show stronger emission compared to the 266 nm excited fluorescence. The two protein samples show a similar pattern and have the highest intensity in the 350 nm band of all the sample materials measured. The two interferents, kaolin and S. Cruentum both show a pattern distinctive from all the other samples marked by particularly low fluorescence in all channels.

#4798 - $15.00 US Received 14 July 2004; revised 7 September 2004; accepted 9 September 2004

Table 2 summarizes the absolute fluorescence cross-sections for individual aerosol particles. The fluorescence cross-sections have been calculated based on the signals measured in the bands centered at 350 nm, 450 nm and 550 nm following 266 nm excitation and in the 450 nm and 550 nm bands following 355 nm excitation. The laser pulse energy was

Table 2. Aerosol samples investigated and estimated fluorescence cross-sections for 266 nm and 355 nm excitation wavelengths in units of cm^2/particle

Sample	***Mean particle size***	***350 nm - 266 nm Excitation***	***450 nm - 266 nm Excitation***	***550 nm - 266 nm Excitation***	***450 nm - 355 nm Excitation***	***550 nm - 355 nm Excitation***
B. Cereus	1.2 μm	1.6E-10	4.0E-12	1.6E-12	4.5E-12	2.0E-12
B. Subtilis	1.0 μm	1.0E-10	2.0E-12	6.5E-13	1.7E-12	6.4E-13
B. Thuringiengis	1.0 μm	4.1E-11	1.2E-12	3.8E-13	9.9E-13	3.5E-13
M. Luteus	1.0 μm	5.0E-11	1.3E-12	6.5E-13	1.2E-12	5.7E-13
B. Megaterium	1.7 μm	1.7E-10	2.8E-12	8.7E-13	4.2E-12	1.3E-12
Brucella Neotomae	1.0 μm	8.9E-11	2.2E-12	7.3E-13	1.4E-12	5.7E-13
Yersinia Rohdei	1.0 μm	1.0E-10	1.8E-11	6.0E-12	1.6E-11	5.2E-12
Pantoea Agglomerans	1.0 μm	6.6E-11	1.9E-11	6.6E-12	1.9E-11	6.0E-12
Ms2 Phage	1.0 μm	2.9E-11	1.5E-11	6.4E-12	1.9E-11	6.9E-12
BG-AFIP	1.0 μm	1.7E-11	3.2E-12	1.7E-12	6.3E-12	3.4E-12
BG -Dugway washed	1.0 μm	8.8E-12	8.9E-13	6.1E-13	3.6E-12	2.6E-12
BG Dugway unwashed	1.0 μm	2.0E-11	2.0E-12	1.2E-12	5.0E-12	3.4E-12
Ova Albumin	1.0 μm	3.7E-10	3.3E-12	5.1E-13	1.9E-12	3.2E-13
Bovine Albumin	1.0 μm	1.7E-10	1.8E-12	4.3E-13	1.4E-12	3.1E-13
Sporisorium Cruentum	5.8 μm	5.8E-12	6.6E-13	2.8E-13	3.2E-12	1.6E-12
Kaolin	1.0 μm	2.4E-12	3.2E-13	4.6E-14	9.5E-13	2.3E-13

measured for both the excitation beams, and their respective beam waist was measured at the focal point of the aerosol chamber to estimate the number of photons incidents on the particle. The number of fluorescent photons emitted by the particle was measured as discussed above for data described in Fig 3. The values in Table 2 are the estimated cross sections for the particle sizes shown. The 266 nm-excited, summed fluorescence cross-sections for the washed vegetative cells are about $1x10^{-10}$ cm^2/cellon average with the majority of the fluorescence occurring in the 350 nm band. The 266 nm-excited fluorescence cross-sections for the bacterial spores average about 1.5 $x10^{-11}$ cm^2/spore. The toxin simulants, ova albumin and bovine serum albumin have the largest 266 nm-excited fluorescence cross sections, $3.7x10^{-10}$ cm^2 and 1.7 x 10^{-10} cm^2 for one μm particles. Our results are in good agreement with the values reported by Faris et al. [14] for dry BG spores. Our cross section results for single, dry B. Subtilis vegetative cells are a factor of seven lower than the cross sections reported by Seaver et al. [15] for cells in liquid suspension. However, Faris et al. also noted a factor of four larger cross section for wet suspensions compared to dry suspensions.

#4798 - $15.00 US Received 14 July 2004; revised 7 September 2004; accepted 9 September 2004

Therefore, our cross section measurements on single particle bioaerosols appear to be in good agreement with results obtained on bulk samples by other investigators.

Differences in the relative intensities of the fluorescence bands shown in Fig. 3 are apparent for different samples, although it is difficult to visually classify them in a systematic manner. As an attempt to show that samples with similar spectral characteristics tend to cluster together, we simplified the data set by co-adding the three emission intensities produced by 266 nm excitation, and the two emission intensities from 355 nm excitation. The fluorescence signals have been normalized to the particle elastic scatter intensity, so that the fluorescence signals are independent of size. Figure 4 plots the summed averaged intensities of the 16 samples shown in Fig. 3 as centroids of ellipses for which the major and minor axes are given by the summed standard deviations for each sample. These ellipses therefore represent approximate probability distributions for the signals obtained from each sample in this simplified two-dimensional projection. This plot illustrates how samples that have significant differences in their response to 266-nm and 355-nm excitations are separated in this data space. Samples that exhibit significantly higher fluorescence following 355-nm excitation are grouped in an elliptical distribution with the major axis aligned, more or less, parallel to the vertical axis. These samples include the bacterial spores, and vegetative cells in

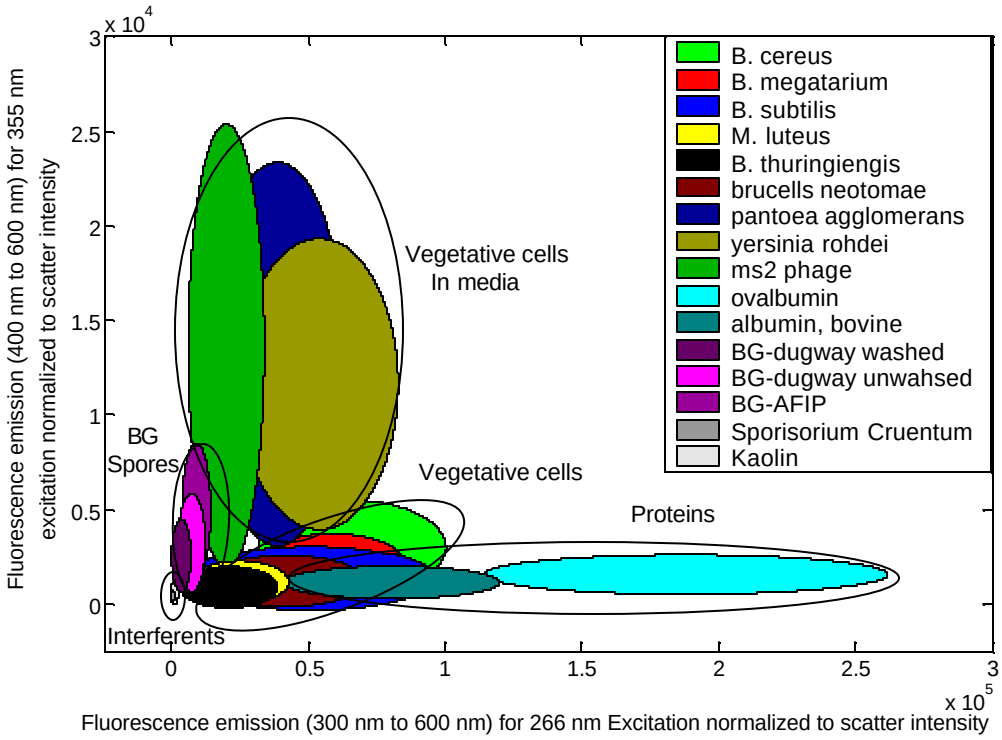

Fig. 4. Scatter plot distribution of the 355 nm-excited fluorescence versus the 266 nm-excited fluorescence for the 16 samples listed in Table 1. The ovals represent the probability that a particle of the indicated type will fall within that range.

media. Signals from the toxin simulants, ova albumin and bovine serum albumin, are dominated by the 266-nm-excited fluorescence and are concentrated along the horizontal axis. Other samples with intermediate fluorescence contributions are clustered between the two extremes. Several samples in this region of the plot are known to contain spent growth media that contributes to the observed fluorescence signal, particularly in the 400 to 600 nm range.

While this initial data set contains a limited number of sample types, and though the quantity of data is not really adequate to justify a more robust analysis, these results are

#4798 - $15.00 US Received 14 July 2004; revised 7 September 2004; accepted 9 September 2004

tantalizing from the point of view of the impact on current bio-aerosol detection. Specifically, there are two features that stand out. First, the small ellipse labeled interferents that occurs near the coordinate origin in Figure 4 includes both kaolin and fungal spores (sporsoruium cruentum). Although easily detected fluorescent signals are routinely recorded from fungal spores, when these are properly normalized to their particle size, the fluorescence from the fungal spores is seen to be clearly distinct from the other bioaerosol sample types. Note that removing either of the excitation wavelengths will lose this clean discrimination. Second, based on the cross sections listed in Table 2, the 355 nm-excited fluorescence cross sections for the BG spores is seen to be larger in the 450 and 550 nm bands than for the 266 nm-excited fluorescence in the same bands. This behavior is unique among the 16 samples investigated in Table 2, and illustrates another way that multiple wavelength excitation provides enhanced discrimination compared to single wavelength approaches.

While these two features may seem minor, they are extremely encouraging from our perspective because they indicate potential for improved discrimination. The major concern for bioaerosol sensing using real time, single particle optical detection methods is not so much of an issue of improving the probability of detection, as it is reducing the probability of false positives. Both of these indicators, the rejection of fungal particles and the improved discrimination of bacterial spores, point to the possibility an improved false positive rate for optical bioaerosol sensing. While it is difficult to project an accurate numerical assessment of the performance improvement based on the limited data shown here; we were frankly surprised to observe even these distinct advantages. These features have stimulated a much stronger effort to acquire significantly larger amounts and types of data with which we can develop a statistically robust measure of effectiveness, such as a confusion matrix, to quantitatively determine the performance advantage of multiple wavelength excitation interrogation. This excitement does not alter our earlier statement that it is unlikely that fluorescence techniques alone will be able to provide species level determination. However, there is much room for improvement in performance to be gained in the space between that lofty goal, and current capability, simply by being able to reject as clutter some of the more common bioaerosols that are now regarded as signature interferents.

Acknowledgments

This work was supported by the DoD chemical and biological defense techbase, administered by the Defense Threat Reduction Agency.

#4798 - $15.00 US Received 14 July 2004; revised 7 September 2004; accepted 9 September 2004